Determination of generalized fracture toughness in composite multimaterial closed corners with two singular terms. Part I: test proposal and numerical analysis.

A. Barroso, D. Vicentini, V. Mantič, F.París

Group of Elasticity and Strength of Materials, School of Engineering, University of Seville, Camino de los Descubrimientos s/n, 41092 Seville, Spain.

Abstract: In the present work a general procedure for the experimental evaluation of Generalized-Fracture-Toughness values at multimaterial closed corners is defined. The lack of symmetries in the stress fields at multimaterial corners with non-isotropic materials makes it extremely difficult to define standard test procedures for Generalized-Fracture-Toughness determination. The proposed procedure is suitable for closed corners (all wedge faces being bonded) having two singular terms. The procedure begins by finding the load configurations at which one of the singular terms in the asymptotic series expansion vanishes, allowing the failure to be controlled by the other, non-vanishing, singular term. An example of a typical bimaterial corner in an adhesively bonded joint with composite materials is extensively analyzed and suitable test configurations for the experimental evaluation of the Generalized-Fracture-Toughness values K_{1C} and K_{2C} associated to the singular terms are defined. The experimental part of this work using a novel modified configuration of the Brazilian Test will be described in a follow up paper.

Keywords: Generalized-Fracture-Toughness, Brazilian test, bimaterial corner, stresses singularities.

1. Introduction

The 2D stress and displacement fields in the neighbourhood of anisotropic multimaterial corners, assuming 2D linear elasticity and a polar coordinate system (r,θ) centred at the corner tip, can be represented by an asymptotic series expansion, with variable separation. See Kondratev [1], Costabel and Dauge [2], Knees and Sändig [3] and Borsuk [4] for a more mathematical approach to the problem. See Wieghardt [5], Williams [6], Vasilopoulos [7], Dempsey and Sinclair [8,9], Sinclair [10,11] and Paggi and Carpinteri [12] for a more applied approach, and Ting [13], Barroso *et al.* [14], Hwu *et al.* [15] and Yin [16] for particular analysis of anisotropic multimaterial corners. Under some simplifying assumptions (e.g. neglecting the possible existence of logarithmic terms) the series expansion for displacements and stresses at a corner tip ($r\rightarrow 0^{+}$) can be written in the following form:

$$\begin{aligned} u_\alpha(r,\theta) &\cong \sum_{k=1}^{n} K_k r^{\lambda_k} g_\alpha^k(\theta) \\ \sigma_{\alpha\beta}(r,\theta) &\cong \sum_{k=1}^{n} K_k r^{\lambda_k - 1} f_{\alpha\beta}^k(\theta) \end{aligned} \qquad (\alpha = r,\theta) \qquad (1)$$

where K_k (k=1,...,n) are the Generalized Stress Intensity Factors (GSIFs), λ_k (k=1,...,n) are the characteristic exponents. If 0<Re(λ_k)<1, 1-λ_k is called the order of stress singularity. Functions $g_\alpha^k(\theta)$ and $f_{\alpha\beta}^k(\theta)$ (k=1,...,n) are the characteristic angular shape functions for displacements ($g_r^k(\theta)$, $g_\theta^k(\theta)$) and stresses ($f_{rr}^k(\theta)$, $f_{\theta\theta}^k(\theta)$, $f_{r\theta}^k(\theta)$) respectively. The angular shape functions $g_\alpha^k(\theta)$ and $f_{\alpha\beta}^k(\theta)$ are normalized according to the definition given in Section 3.1.

The characteristic exponents, λ_k, and angular shape functions, $g_\alpha^k(\theta)$ and $f_{\alpha\beta}^k(\theta)$, depend only on the local geometry, material properties and boundary conditions in a neighbourhood of the corner tip, while the GSIFs, K_k, additionally depend on the far field loading and global geometry. In fact, in the case of proportional loading, the GSIFs K_k are proportional to the load factor.

In geometrical and material configurations where the stress representation given in (1) applies, stress singularities may appear and the GSIFs K_k control the local stress field. If the extension of yielding at the corner tip is small compared to the K-dominated zone (where the stress solution is approximated well by the first singular term, with 0<λ_k<1, in the series expansion (1)) the onset of failure can be assumed to be controlled by critical values of K_k, called Generalized-Fracture-Toughness values, which will be denoted generically in what follows as K_{kC} (see Leguillon and Sanchez-Palencia [17], Leguillon and Siruguet [18], or Henninger and Leguillon [19]).

Unlike the well defined test standards for the experimental determination of fracture toughness values for cracks in homogeneous isotropic materials (K_{IC}, and K_{IIC} respectively for the symmetrical and unsymmetrical cases), the lack of symmetries in the stress fields in general configurations of anisotropic multimaterial corners makes it difficult to develop a general procedure for Generalized-Fracture-Toughness determination in corners of this kind.

The characteristic exponents λ_k and the angular shape functions $g_\alpha^k(\theta)$, $f_{\alpha\beta}^k(\theta)$ in series (1) must be known, and a procedure for evaluating K_k should be available before any proposal of an experimental procedure is attempted. The measurement of any critical GSIFs (K_{kC}) is based on the evaluation of K_k at the experimental failure load when the external load distribution activates only one singular mode. This is the key idea of the proposed procedure.

In this work, the evaluation of λ_k, $g_\alpha^k(\theta)$ and $f_{\alpha\beta}^k(\theta)$ is based on a general analytical procedure proposed in Barroso *et al*. [14] which applies for linear elastic generalized plane strain states, without any limitation in the number and nature of materials. In particular, mathematically degenerate materials in the framework of Stroh formalism of anisotropic elasticity, see for example Ting [20], are covered by this analytical procedure, a feature usually lacking in similar procedures proposed elsewhere. The evaluation of K_k is based on a numerical procedure (Barroso *et al* [21,22]) which has proved to be accurate in most difficult cases with multiple singularities. Examples of characterization in mixed modes at bimaterial interfaces can be found in Dollhofer et al [23].

The aim of the present work is to propose a general procedure for the Generalized-Fracture-Toughness determination in 2D multimaterial anisotropic closed corners having two singular terms. With two singular terms, the evaluation of Generalized-Fracture-Toughness K_{kC} (k=1,2) is based on the possibility of isolating each singular term with a particular external load distribution. Notice that corners having only one singular term present no difficulty as the asymptotic stress state is controlled by only one GSIF, defined, e.g., as K_I whose value at the failure load defines K_{IC}. By contrast, 2D corners having more than two singular terms present additional difficulties as the isolation of each singular term is not always possible (as will be detailed in Section 2).

The procedure presented here is only valid for closed corners (with all materials wedges perfectly bonded, without any external boundaries, sometimes referred to as cross-points) because the proposed procedure is, essentially, based on the well-known Brazilian test (introduced in 1943 almost simultaneously by Carneiro [24] and Akazawa [25]), with the multimaterial corner at the centre of the disk loaded in compression. The compression load is applied in the diametric direction at any generic point along the external perimeter and this is only possible for the case of closed corners. A similar Brazilian disk specimen has been used by Banks-Sills et al. [26,27] in the evaluation of fracture toughness of interface cracks in bimaterial systems, including thermal curing stresses.

Based on a previous work by the same authors, Barroso *et al* [28] and also based on the conclusions obtained by Qian and Akisanya [29], the thermal stresses due to the curing process have not been considered in the present analysis of the bimaterial corner of the Brazilian disk specimen.

Two different test procedures will be detailed in Section 2 while section 3 will present the application of the general procedure developed to a particular bimaterial corner of a real structure.

For a practical illustration of the procedure in the field of composite materials, it has been applied to a particular CFRP-epoxy bimaterial closed corner (CFRP: Carbon-Fiber-Reinforced-Plastic). The experimental results and failure envelope, based on critical values of the GSIFs, will be described in a follow up paper [32]. A similar failure envelope, based on the strain energy release rate instead of GSIFs was presented for adhesively bonded joints by Hafiz et al. [30].

Although the procedure has been applied in the present paper to a bimaterial corner, there is no additional impediment to use it in three- or multi-material corner configurations, provided that the stress representation involves only two singular terms. Examples of composite three-material corners having two stress singularities have been extensively reported in literature, see for example Barroso et al. [31] for the detailed analysis of the three-material corner as that depicted in Figure 1, corner b.

2. Description of the test procedures

Figure 1 shows some examples of multimaterial closed corners appearing in an adhesively bonded joint between a $[0/90]_S$ laminate and aluminium. The bimaterial corner (a) has a 90º wedge of unidirectional carbon fibre reinforced lamina (with the

fibre in the x direction) and a 270º wedge of isotropic adhesive. The three-material corner (b) has a 90º wedge of a unidirectional fibre reinforced lamina (the fibre in the z direction), a 90º wedge of the same material but with the fibre oriented in the x axis and a 180º wedge of isotropic adhesive material. In these two examples, there are no symmetry planes. Figure 1c shows an isotropic bimaterial corner. Finally, Figure 1d shows schematically a generic multimaterial closed corner.

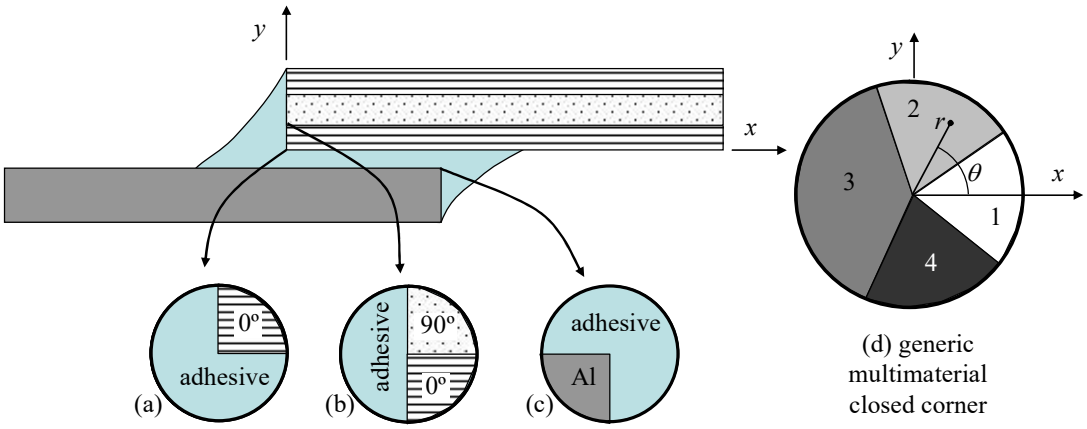

Figure 1. Examples of multimaterial closed corners in a real structure (lap joint).

As mentioned previously in the Introduction, the proposed procedure is essentially based on the Brazilian Test, there being two alternatives which will be explored in Sections 2.1 (uniaxial test) and 2.2 (biaxial test) respectively. In this procedure the test sample is a flat cylinder, such as those shown in Figures 1a, 1b and 1c, which will be subjected to uniaxial or biaxial loading.

As the present procedure is suitable for corner configurations having two singular terms, the following examples will be particularized for the determination of two Generalized-Fracture-Toughness values (K_{1C} and K_{2C}).

2.1. Case with isolated terms. Uniaxial test procedure

The uniaxial test procedure simply consists, in a first step, of the numerical simulation of a Brazilian Test in which the sample is loaded in uniaxial compression, with a load P, as shown in Figure 2a (particularized, as an example, for the bimaterial corner of Figure 1a) at different angles along the external circular perimeter. Assuming linear elastic behaviour and using the appropriate tools for determining the GSIFs (K_k), it is possible to plot the evolution of K_1 and K_2 (under load P) with the angle α (as shown schematically in Figure 2b). Recall that K_1 and K_2 are associated to different values of characteristic exponents λ, therefore having different units (MPa/mm$^{\lambda-1}$).

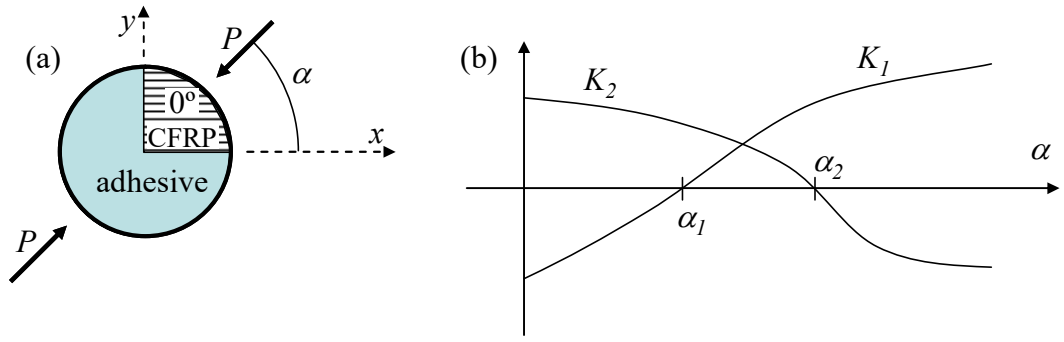

Figure 2. Uniaxial test procedure.

Once a representation like the one shown in Figure 2b is obtained, if both curves, representing the dependencies of K_1 and K_2 (for the external load P) on the angle α, cut the x-axis at angles α_1 and α_2 for K_1 and K_2 respectively, it means that there exist two test configurations in which the singular terms can be isolated (K_1=0 at $\alpha=\alpha_1$ and K_2=0 at $\alpha=\alpha_2$). Thus, in these configurations the local stress fields are only controlled by one singular term (one GSIF value).

The second step of the procedure consists of the experimental testing at these particular angles α_1 and α_2. The failure loads obtained in tests for $\alpha=\alpha_1$ and $\alpha=\alpha_2$ allow the Generalized-Fracture-Toughness values K_{1C} and K_{2C} to be evaluated by simply scaling the values obtained numerically for K_1 and K_2 (for a load value P, Figure 2b) with the obtained failure loads P_1 and P_2 and taking into account the dimensions of the test specimen, see Vicentini et al. [32].

At this point, the previously mentioned difficulty in corners having more than two singular terms in the series expansion (1) is clear. If a third curve, associated to a third singular term, is added to a representation like the one in Figure 2b, the value of this third K_3 at the test orientations α_1 and α_2 will not, generally speaking, be zero. Thus, the isolation of each singular term will not be possible in the present test.

It should be mentioned that the present form does not pretend to propose a physically based analytical expression for an interaction formula of a general mixed mode failure criterion based on GSIFs and their corresponding Generalized-Fracture-Toughness values. This is the reason why several additional load configurations different from those leading to K_1=0 or K_2=0 will be also analyzed and experimentally tested. If the interaction formula were known *a priori*, it would only be necessary to determine K_{1C} and K_{2C} and substitute them in the interaction formula.

Defining a failure criterion in terms of the specimen strength, some size-scale effects will appear. Applying a dimensional analysis, a GSIF can be expressed as (see Leicester [33], Carpinteri [34], Carpinteri and Paggi [35], Dunn *et al* [36] and the references therein):

$$K_k = \sigma_{nom} R^{1-\mathrm{Re}(\lambda_k)} A_k \qquad (k=1,2) \qquad (2)$$

where σ_{nom} is a nominal stress in the problem, R is a characteristic length (the radius in the present case) and A_k is a shape factor taking into account the geometry and material properties of the problem.

A Generalized-Fracture-Toughness based failure criteria could be expressed in a general form as:

$$K = \kappa_C(\psi) \qquad (3)$$

where $K = \sqrt{\left(\frac{K_1}{K_{1C}}\right)^2 + \left(\frac{K_2}{K_{2C}}\right)^2}$ is a normalized GSIF modulus (a dimensionless magnitude) and ψ is a normalized fracture-mode-mixity angle, $\tan\psi = (K_2 / K_{2C})/(K_1 / K_{1C})$. Unlike the traditional mode mixity definition in the case of a crack, $\tan\psi = (K_2 / K_1)$, the inclusion of the fracture toughnesses is due to the different units of K_1 and K_2 in the present case. The parameterization $(\psi, \kappa_C(\psi))$ defines a hypothetical failure envelope curve based on Generalized-Fracture-Toughness concepts. It should be stressed that using (2) and (3) an explicit expression of the size-scale effect on the specimen strength (e.g. in terms of the critical nominal stress σ_{nom}) can easily be deduced.

2.2. Case of non-isolated terms. Biaxial test procedure

If neither of the curves cuts the x-axis, see for example Figure 3a, a second alternative is to perform a biaxial test. In the hypothetical case of Figure 3a, which is obtained as indicated in Section 2.1, the biaxial test loading for isolating the first singular term K_1 may be defined using the following procedure.

Let the values of K_2 considering a unit load P=1, at orientations α=0º and α=90º, be K_2=H_1 and H_2, respectively. Then, the biaxial test configuration would consist in a compression loading of a generic value P at α=0º and a tensile loading of value $(H_1/H_2)\cdot P$ at α=90º. In this situation, for a load P, and applying the superposition principle, the compression load would contribute by K_2=$H_1\cdot P$ and the tensile load would contribute by K_2=- $H_2\cdot(H_1/H_2)\cdot P$=-$H_1\cdot P$, leading to a superposed total value of K_2=0. In this way the first singular term governed by K_1 has been isolated.

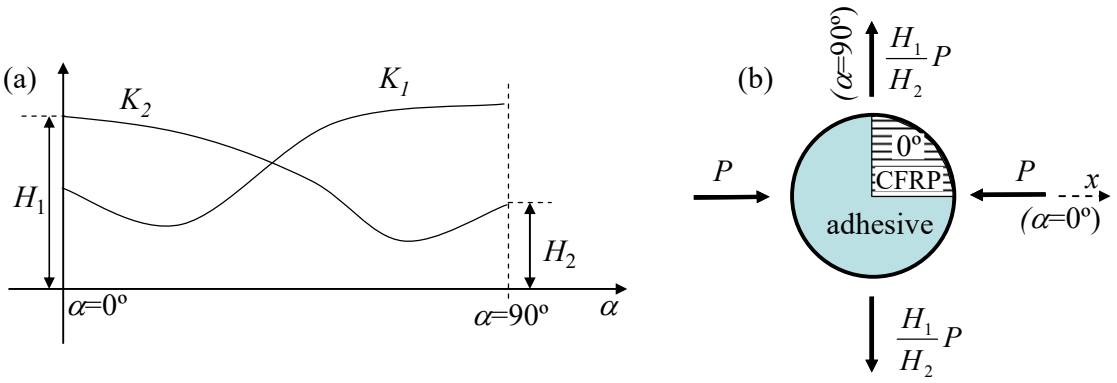

Figure 3. Biaxial test procedure.

The same procedure should also be used to isolate the second singular term governed by K_2 in case no load orientation makes K_1 to vanish, as schematically depicted in Figure 3a.

The critical point of this alternative hinges on the difficulty of the practical application of a tensile load in the Brazilian test sample. An additional fixture or device can be bonded at the corresponding angle, but the adhesive bonding of this device should have a greater strength than that of the actual corner which is being measured. It should also be taken into account that the size of the bonded device, at the boundary of the sample, should be small in comparison with the sample radius. The reason is to avoid, in view of the Saint-Venant's Principle, a change in the stress state of the sample centre induced by the concentrated load considered in the numerical model used to obtain the results of Figure 3a.

Note that, in the case of GSIF dependencies as shown in Figure 2, the biaxial test is also applicable, and easy to perform experimentally, as it would involve only two uniaxial compressions.

3. Application to a real bimaterial closed corner

3.1. Evaluation of stress singularities and angular shape functions

The procedures introduced above will be applied to the bimaterial corner shown in Figure 1a. The calculation of the orders of stress singularities and angular shape functions in (1) can be obtained by the familiar techniques, see for example Ting [13], Barroso *et al*. [14], Hwu *et al*. [15] or Yin [16] among others. Specifically, the procedure by Barroso *et al*. [14] has been used in the present work. The values of the three smallest non-trivial characteristic exponents (λ_1, λ_2, λ_3) obtained are shown in Figure 4, where the mechanical properties of the materials considered in the corner are also included. The bimaterial closed corner under analysis has two singular terms, as $\lambda_3>1$. An additional third (regular) term has also been calculated, as suggested in Barroso *et al*. [37], to accurately represent the stresses and displacements near the corner tip. In any case, as will be seen later, the contribution to the asymptotic stress field in the reasonably small neighbourhood of the corner is dominated by the two singular terms appearing in this particular configuration.

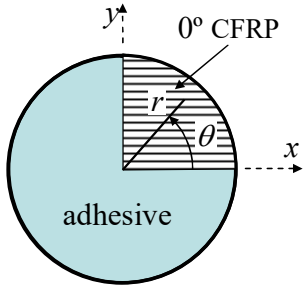

Composite (AS4/8552)
E_{11}=141.3 GPa, E_{22}=E_{33}=9.58 GPa
G_{12}=G_{13}=5.0 GPa, G_{23}=3.5 GPa
ν_{12}=ν_{13}=0.3, ν_{23}=0.32

Adhesive FM-73M.06
E=3.0 GPa, ν=0.35

Characteristic exponents
λ_1=0.763236
λ_2=0.889389
λ_3=1.106980

Figure 4. Properties and characteristic exponents (λ_k) of the bimaterial closed corner.

By substituting the computed values of λ_k in (1), the asymptotic displacement and stress representations can be particularized as follows:

$$u_\alpha(r,\theta) \cong K_1 r^{0.763236} g_\alpha^1(\theta) + K_2 r^{0.889389} g_\alpha^2(\theta) + K_3 r^{1.106980} g_\alpha^3(\theta)$$
$$\sigma_{\alpha\beta}(r,\theta) \cong \frac{K_1}{r^{0.236764}} f_{\alpha\beta}^1(\theta) + \frac{K_2}{r^{0.110611}} f_{\alpha\beta}^2(\theta) + K_3 r^{0.106980} f_{\alpha\beta}^3(\theta) \quad (4)$$

where it is clear that the third term of the stress representation tends to zero when $r \to 0$, the singular character of stresses being associated to the first two singular terms. In the case of u_θ an additional term $K_r \cdot r$ needs to be added to the displacement representation in order to include the rigid body rotation. This term can be avoided if the boundary conditions of the numerical model (FEM or BEM) impose a null rotation at the corner tip, an effect which it is not always possible to obtain. The terms associated to the rigid body translation have not been included in (4) as relative displacements with respect to the corner tip were used in the numerical procedure for K_k evaluation.

The characteristic angular shape functions can also be computed from the semianalytic expressions given by Barroso *et al.* [14]. For the particular corner under study, they have been included in the Appendix (Figures A1, A2 and A3, and Tables A1, A2 and A3 for the first three terms, respectively). The GSIFs have been standardized following the procedure by Pageau *et al*. [38] giving rise to expressions of the angular shape functions which fulfil the condition $f_{\theta\theta}^k(\theta = 0^\circ) = (2\pi)^{\lambda_k - 1}$ (k=1,2,3), in order to obtain:

$$\sigma_{\theta\theta}(r,\theta = 0^\circ) = \sum_{k=1}^{3} \frac{K_k}{(2\pi r)^{1-\lambda_k}} \quad (5)$$

The K_k values have dimensions of MPa·mm$^{1-\lambda}$, $f_{\alpha\beta}(\alpha,\beta=r,\theta)$ being dimensionless and $g_\alpha(\alpha=r,\theta)$ having dimensions of MPa^{-1}. In the numerical examples of the following sections only normalized values of K_k will be used.

3.2. Numerical results for the uniaxial test

The GSIFs K_k (k=1,2,3) for the particular corner under study have been extracted from FEM results using the postprocessing procedure by Barroso *et al.* [21,22]. In this procedure, the determination of K_k is based on the minimization of the sum of quadratic differences between the analytical series expansion (4) and numerically computed displacements at common bonded interfaces (θ=0º, 90º) by a simple and robust least squares technique. Any other available technique could be used for evaluating the GSIFs.

At these common edges, 22 nodes in the range $0.00057 \cdot R < r < 0.00162 \cdot R$ have been used for the K_k determination, where R is the specimen radius. Figure 5 shows the Finite Element model (FEM) used for the problem, in which a regular mesh has been used, with nodes of radial lines, each of 5º, and 200 nodes along each radial line with a progressive refinement of the mesh towards the corner tip, where the final element size is $7.4 \cdot 10^{-5} \cdot R$. The load used in the FEM model was 100N.

Plane elements with 4 nodes and 2 degrees of freedom (u_x, u_y) have been used with the plane strain option. In a previous work (Barroso *et al*. [39]), it was found that the stress

state at the free edges was less severe than that at the interior of the specimen, for which reason the plane strain option was chosen. Boundary conditions in displacements have been used to avoid rigid body motions. The CFRP solid was modelled as an equivalent linear elastic orthotropic material and the adhesive as a linear elastic isotropic material, whose properties were introduced in Figure 4.

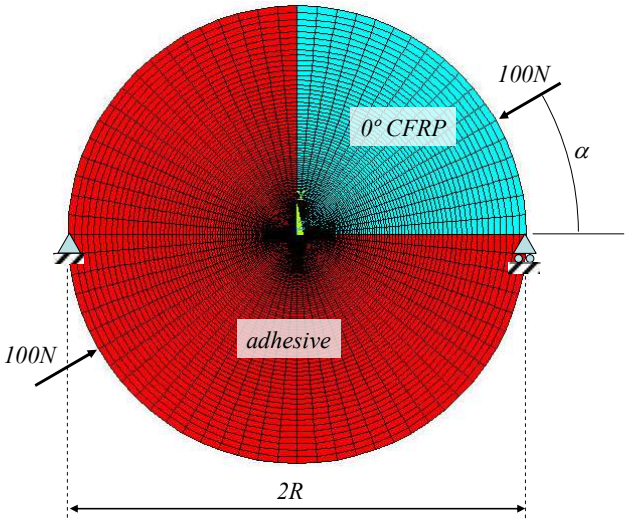

Figure 5. FEM model of the bimaterial corner problem

The normalized values, according to Pageau *et al*. [38], of the GSIFs associated to the two singular terms (K_1, K_2) for 0º<α<180º are shown in Figure 6, where it can be observed that $\alpha \approx 13º$ and $\alpha \approx 60º$ are the test configurations at which K_2 and K_1 respectively vanish.

It can be observed from Figure 6 that there are two load orientations for which K_1 and K_2 vanish respectively (α≈60º and α≈143º for K_1 and α≈13º and α≈115º for K_2). These four cases have to be analyzed, as well as additional cases in which none of the GSIFs vanishes to determine a large number of points in the failure envelope. Obviously, the choice of α≈60º or α≈143º will lead to different values of K_{1C} (which might be denoted as $K_{1C}^{+} > 0$ and $K_{1C}^{-} < 0$), which is conceptually acceptable, as both values correspond to different stress states. Nevertheless, any particular choice will have no relevant influence on the shape of the failure envelope (which is obtained in the experimental part of the present work, which will be described in a follow up paper (Vicentini et al. [32]). In any case, it should be mentioned that the selected angles, $\alpha \approx 13º$ and $\alpha \approx 60º$ correspond to maximum values of the non vanishing GSIF, a fact which may slightly increase the accuracy of K_{kC} estimations.

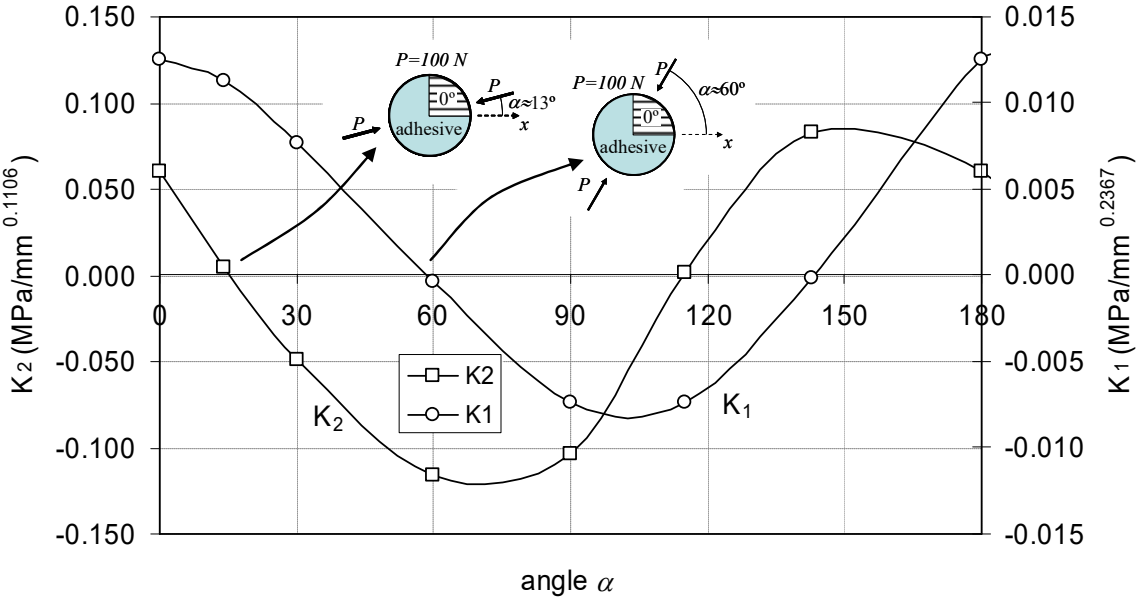

Figure 6. Standardized values of K_1 and K_2 in the uniaxial test configuration.

It must be stressed that due to the fact that the values of the GSIFs are normalized, the relative influence of GSIFs on the stress distribution depends not only on the absolute values of GSIFs, shown in Figure 6, but also on the values of angular shape functions and the specific distance from the corner tip. This fact can be further clarified by representing stresses and displacements for the particular case of α=13º, where K_1=0.01125, K_2=0.007319 and K_3=0.01266. In this particular case the normalized value of K_2 is only ~1.5 times lower than the absolute value of K_1, and K_3 (which is not associated to a singular term) is higher than K_1.

Introducing these values into (4) the displacements and stresses are shown, at r=0.001·R, in Figures 7 (u_r, u_θ) and 8 (σ_θ, $\sigma_{r\theta}$, σ_r) together with the FEM results obtained. In Figures 7-8, not only the total displacement and stress components are shown but also the individual contribution of each one of the terms of the series expansion (4). Despite the values of the normalized GSIFs obtained for α=13º (K_1=0.01125, K_2=0.007319 and K_3=0.01266), it can be clearly observed in Figures 7-8 that the displacement and stress fields are almost exclusively determined by the first term of the series expansion (4), the second and third term contributions being almost negligible.

The difference in the displacement component u_θ observed in Figure 7b is associated to a rigid body rotation, which has been taken into account in (4) as an independent term, $K_r \cdot r$, the difference thus being constant all along the circumferential coordinate θ.

a)

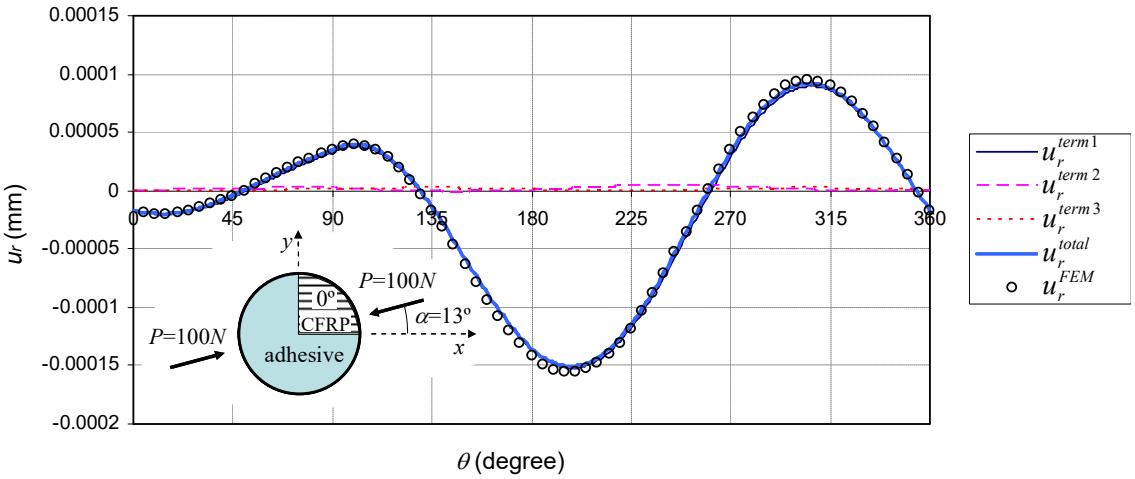

b)

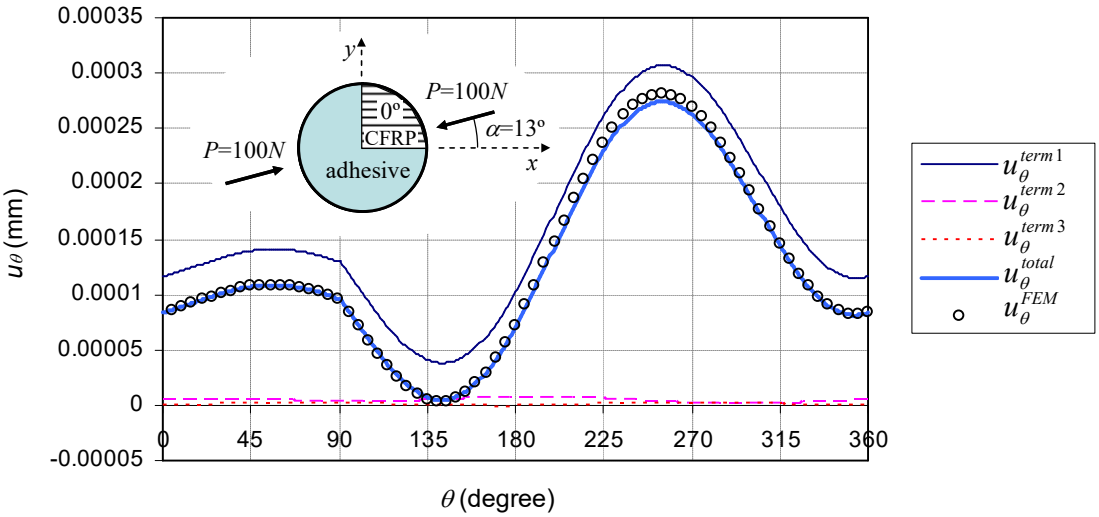

Figure 7. FEM and series expansion results, a) u_r and b) u_θ, for α=13° at r=0.001·R.

a)

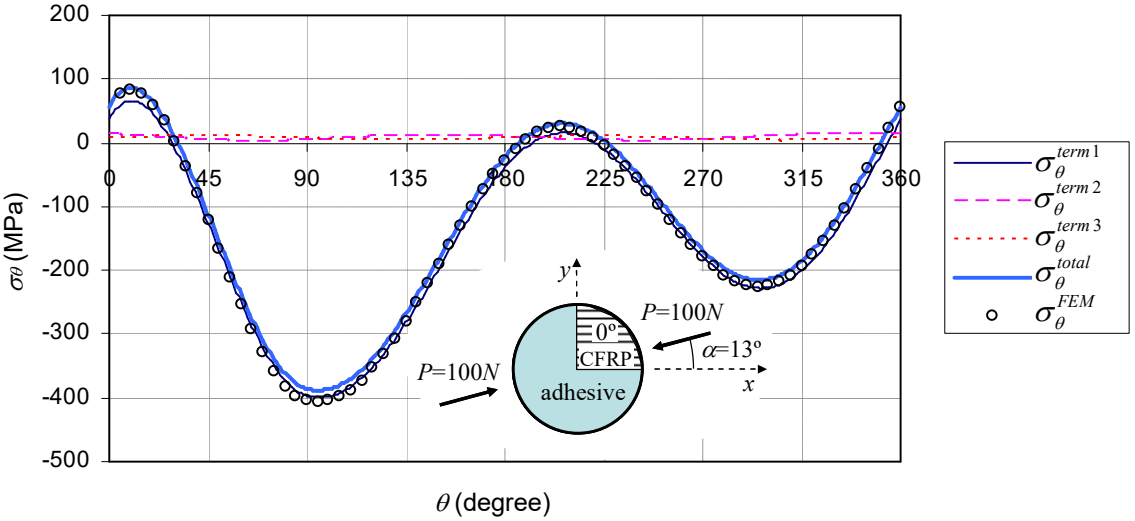

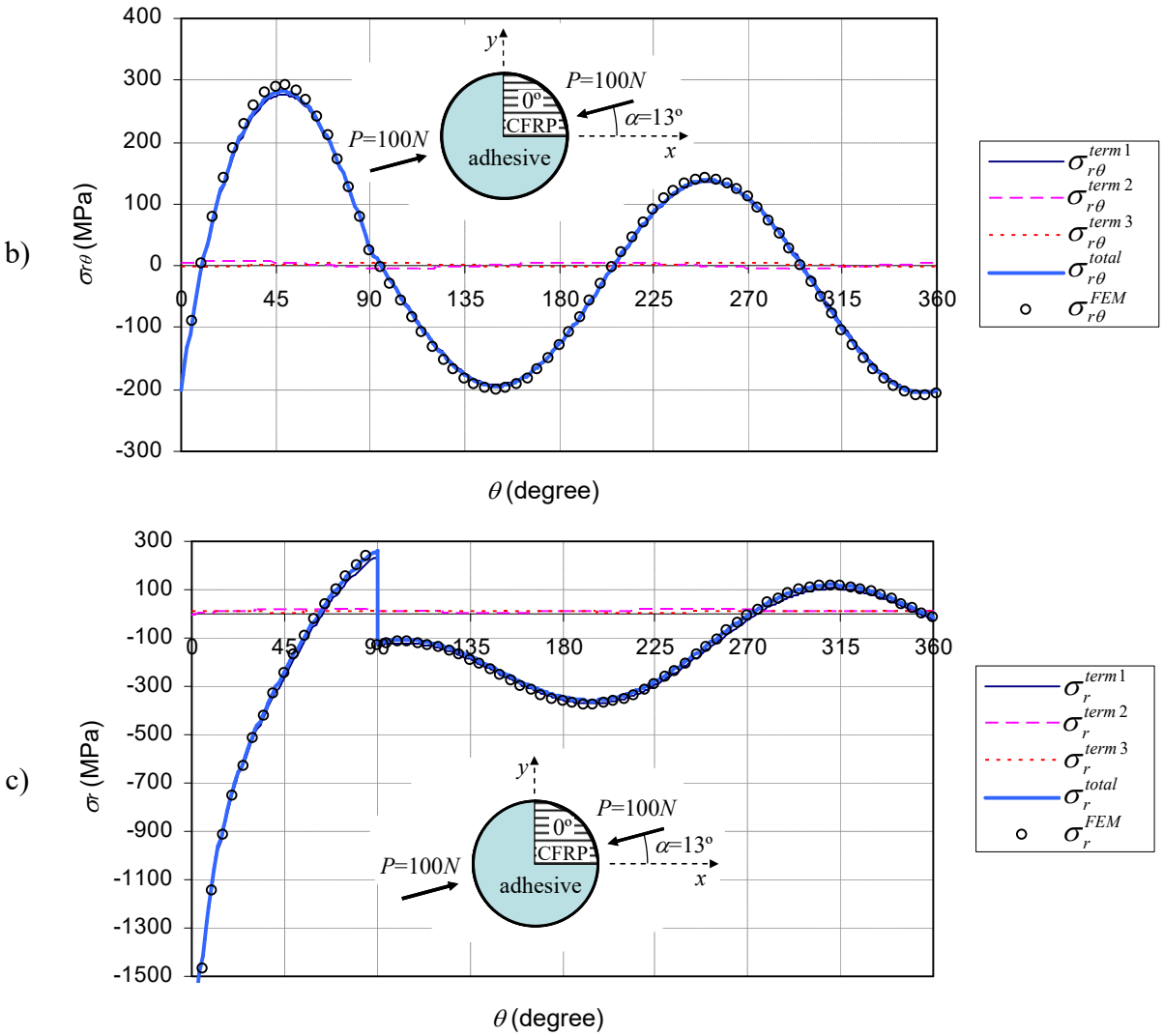

Figure 8. FEM and series expansion results, a) σ_θ, b) $\sigma_{r\theta}$, c) σ_r, for α=13º at r=0.001·R.

As can be observed in Figure 8c, σ_r is not continuous neither at θ=90º nor θ=0º and 360º, where the material changes and the perfect adhesion conditions do not require the continuity of this stress component.

Although only displacements have been used in the postprocessing procedure extracting the values of K_k from FEM results, the fitting between the numerical (FEM) and the series expansion results in stresses (Figure 8) is also excellent.

In the test configuration at which K_1=0 ($\alpha\approx$60º), Figures 9-10 show the displacements and stresses in a similar way to Figures 7-8 for the case K_2=0.

Both singular terms in the present configuration are weak singularities with $0.5<\lambda_k<1$, but the second one, considered now (K_1=0) is particularly weak λ_2=0.889389. Thus, although still having the unique singular term (the second) as the most important contribution to the total displacement and stress fields at the chosen distance r=0.001R, the first regular term with λ_3=1.106980 sometimes shows a relatively significant contribution, as will be observed later on.

With reference to the displacement components u_r, u_θ and also to the shear stress $\sigma_{r\theta}$, Figures 9 and 10b respectively, the situation is similar to the one observed in the previous case, ($K_2 \approx 0$, α=13º), with the non-vanishing singular term (K_2 in this case, K_1 in the previous one) having almost all the weight of the corresponding displacements and stress components.

The difference in the u_θ component is, as in the previous case, Figure 7b, associated to the rigid body rotation which has been taken into account in (4) as $K_r \cdot r$. In the case of σ_θ and σ_r (Figures 10 a and c) the contribution of the regular term to the maximum total stress value is not negligible, it being lower than 10%. Thus, in this case, the critical value of K_2 at failure should be considered only a good estimation of the real K_{2C}. The real value might be slightly lower or slightly higher depending on the contribution of the non-vanishing terms to the failure.

a)

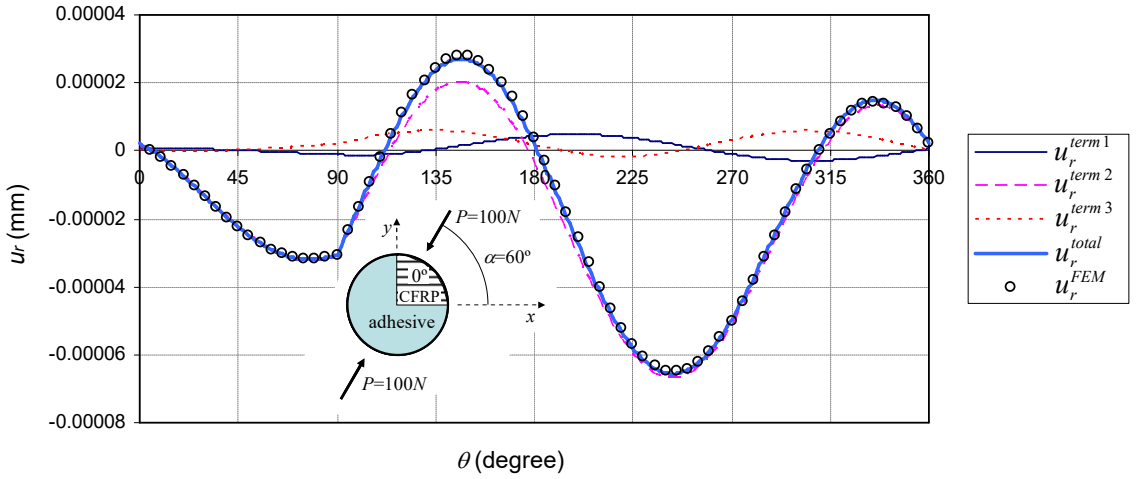

b)

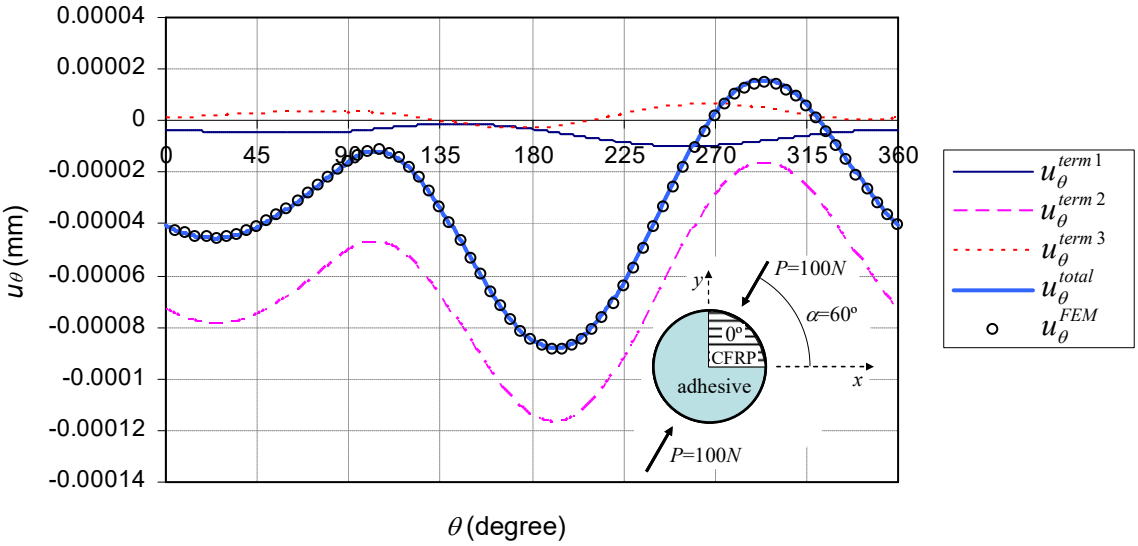

Figure 9. FEM and series expansion results, a) u_r and b) u_θ for α=60º at r=0.001·R.

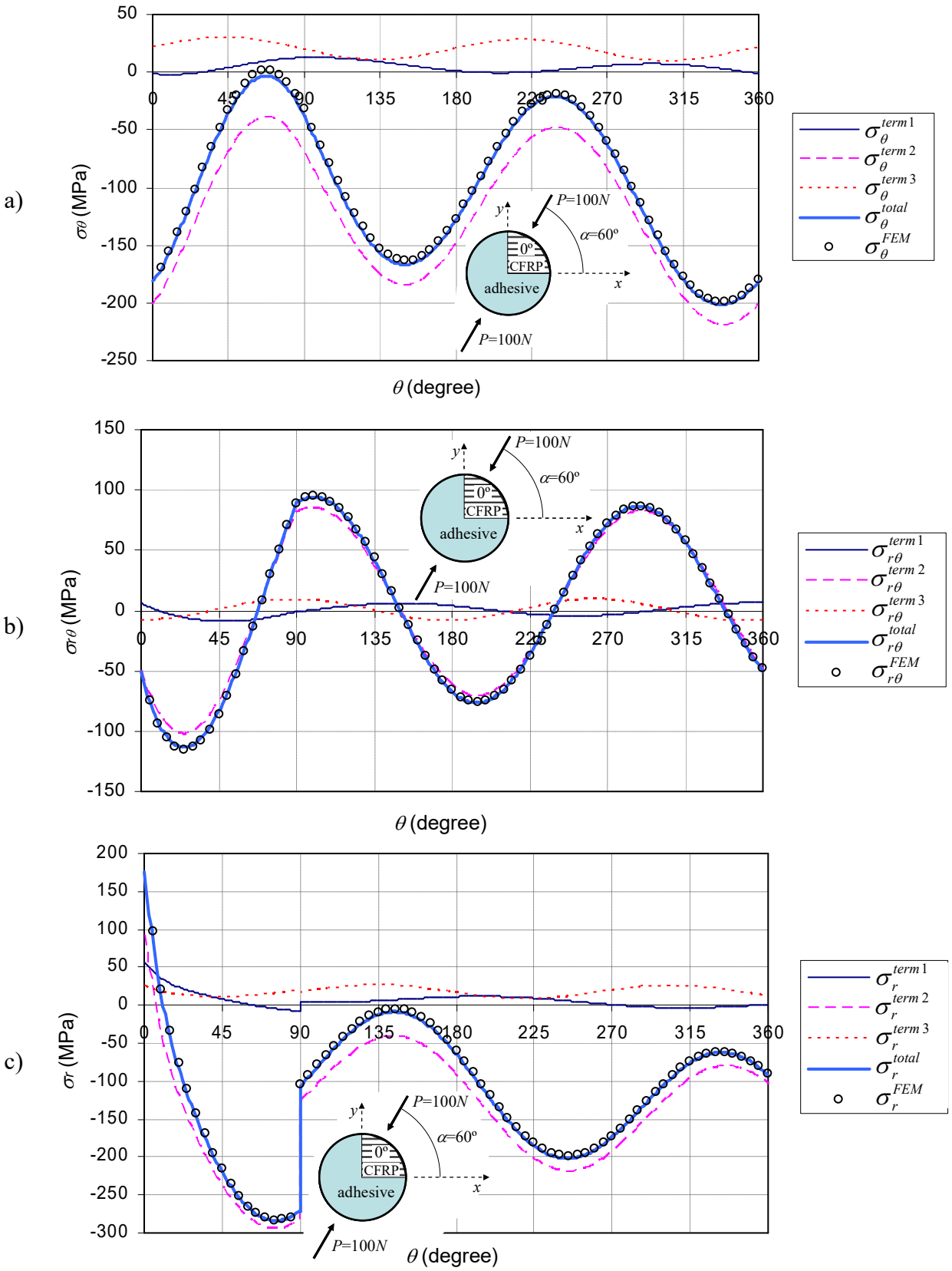

Figure 10. FEM and series expansion results, a) σ_θ, b) $\sigma_{r\theta}$, c) σ_r, for α=60º at r=0.001·R.

In Figure 10c, as already observed in Figure 8c, σ_r is not continuous neither at θ=90º nor θ=0º and 360º.

To sum up, having a configuration in which one of the singular terms is negligible ($\alpha\approx$13º for $K_2\approx0$ and $\alpha\approx$60º for $K_1\approx0$) permits the determination of the critical values of the GSIFs (K_{1C} and K_{2C} respectively) by simply evaluating the K_k value at the experimentally obtained failure load.

3.3. Definition of the biaxial tests

Using the results shown in Figure 6, in particular the values of K_1 and K_2 associated to the load orientations α=0º and α=90º, it is possible to define two biaxial test configurations having either K_1=0 or K_2=0. The values of K_1 and K_2 from Figure 6 and the procedure introduced in Section 2.2, suggest the two test configurations shown in Figure 11a and b, to isolate the singular terms associated to K_2 and K_1 respectively, by means of the superposition principle.

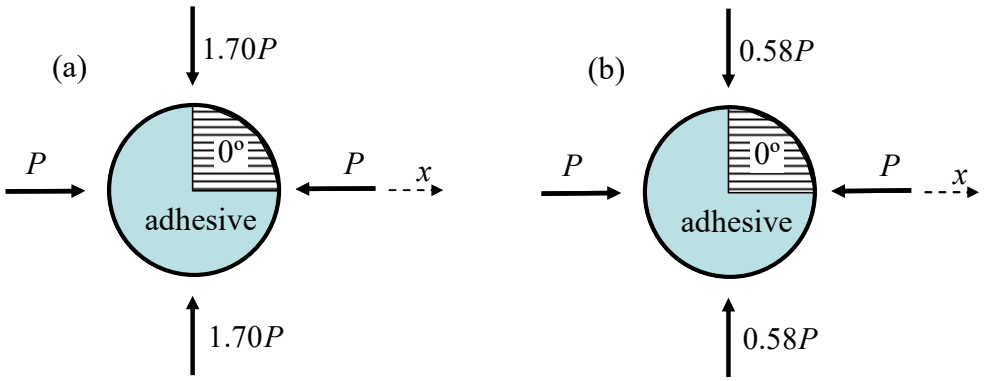

$$K_1 = K_1^{0^\circ} + 1.70K_1^{90^\circ} = 0 \qquad K_2 = K_2^{0^\circ} + 0.58K_2^{90^\circ} = 0$$

Figure 11. Biaxial test configurations for: a) K_1=0 and b) K_2=0.

The coefficients 1.70 (Figure 11a) and 0.58 (Figure 11b) have been obtained by simply dividing the values of K_1 and K_2 associated respectively to α=0º and α=90º.

5. Conclusions

In the present work an experimental test procedure has been developed for Generalized-Fracture-Toughness determination in multimaterial closed corners having two stress singularities. The procedure is based on a kind of Brazilian disk specimen applied to the corner geometry, for which reason the procedure is only valid for closed corners, which can be loaded in compression at any position along the whole external perimeter.

The procedure is especially suitable for non-symmetric multimaterial corners involving isotropic and non-isotropic materials and having two singularities. The procedure is able to isolate any of the singular modes, which is not possible with standard test procedures for homogeneous isotropic materials, due to the lack of symmetries of the stress states at these corners with non-isotropic materials.

The procedure has been applied to a particular bimaterial corner, typically appearing in adhesive joints involving composites, and the test configurations suitable for the experimental evaluation of the Generalized-Fracture-Toughness values K_{1C} and K_{2C} have been defined.

Once the tests have been carried out and the Generalized-Fracture-Toughness values calculated, a failure envelope can be obtained by testing the samples at different angles, which originate mixed mode stress states. This experimental part will be described in a follow up paper. The present work also shows the influence of the specimen size (the radius) on the specimen strength.

6. Acknowledgements

This work was supported by Junta de Andalucía and European Social Fund through the Projects of Excellence P08-TEP-4071 and P08-TEP-4051, by Ministerio de Ciencia e Innovación through project MAT2009-14022 and also by CAPES Brazilian Ministry of Education for a Doctoral Fellowship for Ms. Daniane Vicentini.

7. References

[1] Kondratev VA. Boundary-value problems for elliptic equation with conical or angular points. Trans Moscow Math Soc 1967; 16: 227–313.
[2] Costabel M. and Dauge M. Construction of corner singularities for Agmon–Douglis–Niremberg elliptic systems. Math Nachr 1993; 162: 209–37.
[3] Knees D and Sändig AM. Regularity of Elastic Fields in Composites. In: Multifield Problems in Solid and Fluid Mechanics. Helmig R, Mielke A and Wohlmuth B. (Eds.), Lecture Notes in Applied and Computational Mechanics 2006; 28: 331-360. Springer.
[4] Borsuk M. Transmission Problems for Elliptic Second-Order Equations in Non-Smooth Domains, Springer, Basel, 2010.
[5] Wieghardt K. Über das spalten und zerreissen elastischer körper. Z Math Phys 1907; 55: 60–103.
[6] Williams ML. Stress singularities resulting from various boundary conditions in angular corners of plates in extension. J Appl Mech 1952; 19: 526-528.
[7] Vasilopoulos D. On the determination of higher order terms of singular elastic stress fields near corners. Numer Math 1988; 53: 51-95.
[8] Dempsey JP and Sinclair GB. On the singular behaviour at the vertex of a bimaterial wedge. J Elasticity 1981; 11: 317-327.
[9] Dempsey JP and Sinclair GB. On the stress singularities in the plane elasticity of the composite wedge. J Elasticity 1979; 9: 373-391.
[10] Sinclair GB. Stress singularities in classical elasticity-I: Removal, interpretation and analysis. Appl Mech Rev 2004; 57: 251-297.
[11] Sinclair GB. Stress singularities in classical elasticity-II: Asymptotic identification. Appl Mech Rev 2004; 57: 385-439.
[12] Paggi M and Carpinteri A. On the stress singularities at multimaterial interfaces and related analogies with fluid dynamics and diffusion. Appl Mech Rev 2008; 61: 020801, 1-22.

[13] Ting TCT. Stress singularities at the tip of interfaces in polycrystals. Damage and Failure of Interfaces, Rossmanith H.P. (Ed.), Balkema, Rotterdam 1997: 75-82.
[14] Barroso A, Mantič V and París F. Singularity analysis of anisotropic multimaterial corners. Int J Fracture 2003; 119: 1-23.
[15] Hwu C, Omiya M and Kishimoto K. A key matrix N for the stress singularity for the anisotropic elastic composite wedges. JSME Int J A-Solid M 2003; 46 (1): 40-50.
[16] Yin WL. Anisotropic elasticity and multi-material singularities. J Elasticity 2003; 71: 263-292.
[17] Leguillon D and Sanchez-Palencia E. Fracture in heterogeneous materials, weak and strong singularities. In: New advances in Computational Structural Mechanics, Ladeveze P. and Zienkiewicz O.C. (Eds). 1992: 423-434.
[18] Leguilon D and Siruguet K. Finite fracture mechanics - Application to the onset of a crack at a bimaterial corner. IUTAM Symposium on Analytical and Computational Fracture Mechanics of Non-Homogeneous Materials 2002:11-18.
[19] Henninger C and Leguillon D. Adhesive fracture of an epoxy joint under thermal and mechanical loadings. J Therm Stresses 2008; 31: 59-76.
[20] Ting TCT. Anisotropic Elasticity: Theory and Applications. Oxford University Press, 1996.
[21] Barroso A, Toro P, Mantič V and París F. Evaluation of generalized stress intensity factors in anisotropic elastic multimaterial corners. In: Proceedings of the 11th European Conference on Composite Materials 2004. Rhodes (Greece).
[22] Barroso A, Graciani E, Mantič V and París F. A least squares procedure for the evaluation of multiple generalized stress intensity factors at 2D multimaterial corners by BEM. Eng Anal Bound Elem (in press) 2011.
[23] Dollhofer J, Beckert W, Lauke B and Schneider K. Fracture mechanical characterization of mixed-mode toughness of thermoplast/glass interfaces. Comp Mater Sci 2000; 19: 223-228.
[24] Carneiro FLLB. A new method to determine the tensile strength of concrete. In: Proceedings of the 5th meeting of the Brazilian Association for Technical Rules 1943: 126-129.
[25] Akazawa T. Méthode pour l'essai de traction de bétons. Journal of the Japanese Civil Engineering Institute (1943), republished in French by the Bulletin RILEM 16 Paris (1953), 13-23.
[26] Banks-Sills L, Travitzky N, Ashkenazi D and Eliasi R. A methodology for measuring interface fracture toughness of composite materials. Int J Fracture 1999; 99: 143–161.
[27] Banks-Sills L, Konovalov N and Fliesher A. Comparison of two- and three-dimensional analyses of interface fracture data obtained from Brazilian disk specimens. Int J Struct Integrity 2010; 1: 20-42.
[28] Barroso A, Vicentini D, París F and Mantič V. Representativity of thermal stresses in designing composite joints based on singular stress states at multimaterial corners. Compos Part A-Appl S 2011; 42:1084-1092.
[29] Qian Z and Akisanya AR. An experimental investigation of failure initiation in bonded joints. Acta Mater. 1988; 46: 4895-4904.
[30] Hafiz TA, Abdel Wahab MM, Crocombe AD and Smith PA. Mixed-mode fracture of adhesively bonded metallic joints under quasi-static loading. Eng Fract Mech 2010; 77: 3434-3445.

[31] Barroso A, Mantič V and París F. Computing stress singularities in transversely isotropic material corners by menas of explicit expressions of the orthonormalized Stroh-eigenvectors. Eng Fract Mech 2009c; 76: 250-268.
[32] Vicentini D, Barroso A, Justo J, Mantič V and París F. Determination of generalized fracture toughness in composite multimaterial closed corners with two singular terms. Part II: experimental results. Eng Fract Mech (submitted for publication) 2011.
[33] Leicester RH, Application of linear fracture mechanics to notched timber elements. Prog Struct Engng 2006; 8: 29-37.
[34] Carpinteri A, Stress-singularity and generalized fracture toughness at the vertex of re-entrant corners. Eng Fract Mech 1987; 26: 143-155.
[35] Carpinteri A and Paggi M. Influence of the intermediate material on the singular stress field in tri-material junctions. Mat Sci 2006; 42: 95-101.
[36] Dunn ML, Suwito W, Cunningham S and May CW, Fracture initiation at sharp notches under mode I, mode II, and mild mixed mode loading. Int J Fracture 1997; 84: 367-381.
[37] Barroso A, París F and Mantič V. Representativity of the singular stress state in the failure of adhesively bonded joints between metals and composites. Compos Sci Technol 2009a; 69: 1746-1755.
[38] Pageau SP, Gadi KS, Biggers Jr. SB and Joseph PF. Standardized complex and logarithmic eigensolutions for n-material wedges and junctions. Int J Fracture 1996; 77: 51-76
[39] Barroso A, Vicentini D, Mantič V and París F. 3D edge effects in adhesive CFRP-Al double-lap joints. Proceedings of the COMATCOMP-09, San Sebastián 2009b: 923-926.

Appendix A: Angular shape functions $g_{\alpha}^{k}(\theta)$, $f_{\alpha\beta}^{k}(\theta)$, ($k$=1,2,3), ($\alpha,\beta$=$r,\theta$)

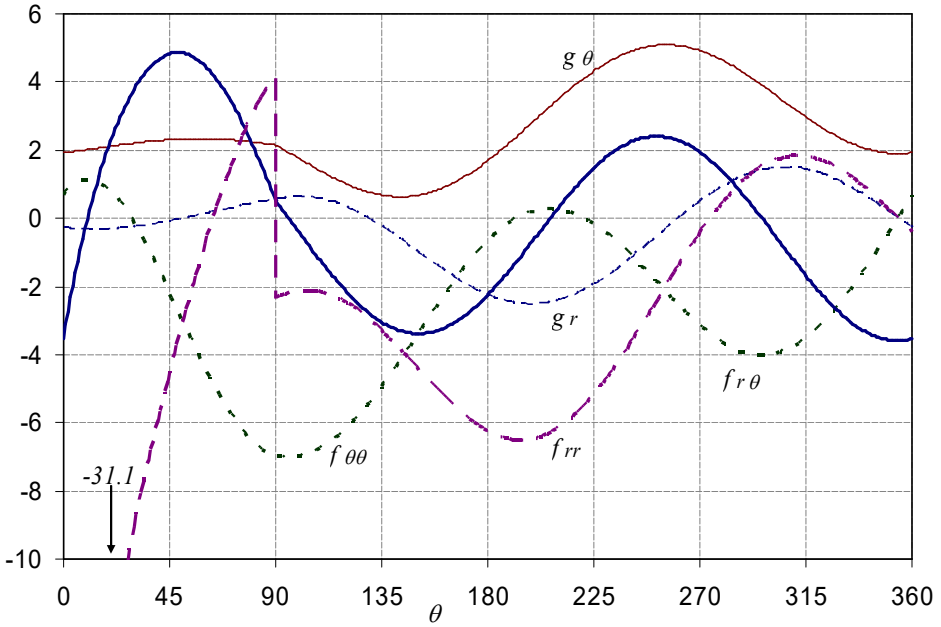

Figure A1. Angular shape functions associated to λ_1 in (1) $g_r^1(\theta)$, $g_\theta^1(\theta)$, $f_{\theta\theta}^1(\theta)$, $f_{r\theta}^1(\theta)$ and $f_{rr}^1(\theta)$ ($f_{\alpha\beta}$ is dimensionless and g_a has dimensions of MPa^{-1}).

θ	g_r (MPa^{-1})	g_θ (MPa^{-1})	$f_{\theta\theta}$	$f_{r\theta}$	f_{rr}
0	-0.2891	1.9311	0.6472	-3.5404	-31.1077
15	-0.3299	2.0661	1.0618	1.2386	-15.7554
30	-0.2566	2.2091	-0.1616	3.7880	-9.0372
45	-0.0880	2.3092	-2.2054	4.8281	-4.5299
60	0.1298	2.3353	-4.4043	4.4767	-0.7570
75	0.3510	2.2790	-6.1512	2.9151	2.2468
90	0.5378	2.1512	-6.9653	0.5120	4.1729
91	0.5540	2.1125	-6.9796	0.4213	-2.3127
105	0.6099	1.5486	-6.8815	-0.8791	-2.1141
120	0.3262	1.0078	-6.1720	-2.1517	-2.4722
135	-0.2448	0.6813	-4.9536	-3.0461	-3.3061
150	-0.9739	0.6748	-3.4464	-3.3816	-4.3970
165	-1.6979	1.0256	-1.9282	-3.0938	-5.4688
180	-2.2540	1.6939	-0.6765	-2.2489	-6.2457
195	-2.5137	2.5716	0.0899	-1.0290	-6.5107
210	-2.4099	3.5047	0.2558	0.3054	-6.1506
225	-1.9511	4.3251	-0.1658	1.4703	-5.1803
240	-1.2193	4.8860	-1.0369	2.2177	-3.7399
255	-0.3534	5.0925	-2.1237	2.3873	-2.0655
270	0.4804	4.9213	-3.1454	1.9402	-0.4402
285	1.1227	4.4254	-3.8334	0.9671	0.8653
300	1.4547	3.7232	-3.9879	-0.3308	1.6486
315	1.4230	2.9735	-3.5194	-1.6839	1.8180
330	1.0503	2.3421	-2.4684	-2.8103	1.4114
345	0.4309	1.9674	-0.9964	-3.4754	0.5878
360	-0.2891	1.9311	0.6472	-3.5404	-0.4058

Table A1. Values for the normalized angular shape functions associated to λ_1 in (1) $g_r^1(\theta)$, $g_\theta^1(\theta)$, $f_{\theta\theta}^1(\theta)$, $f_{r\theta}^1(\theta)$ and $f_{rr}^1(\theta)$.

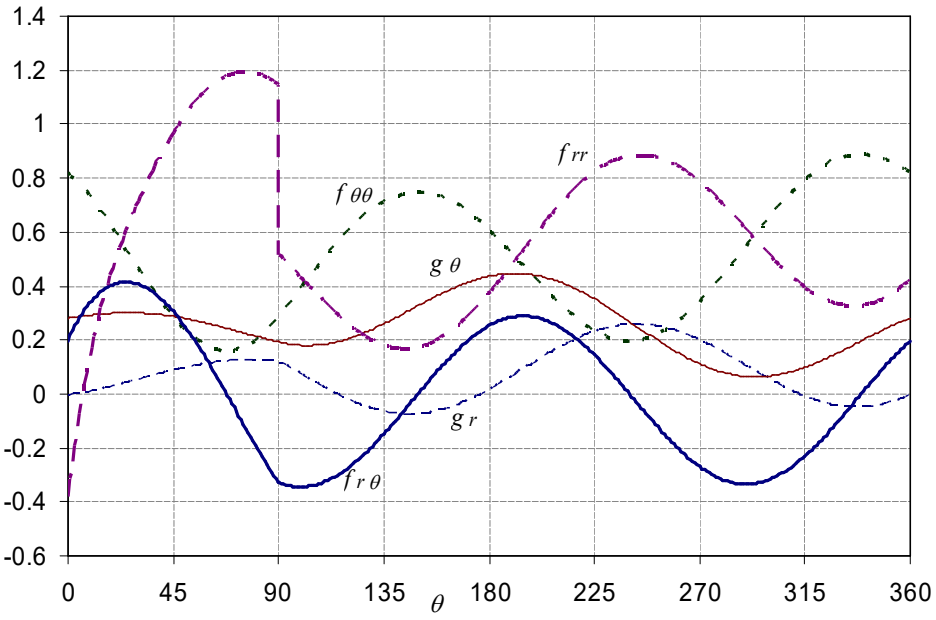

Figure A2. Angular shape functions associated to λ_2 in (1) $g_r^2(\theta)$, $g_\theta^2(\theta)$, $f_{\theta\theta}^2(\theta)$, $f_{r\theta}^2(\theta)$ and $f_{rr}^2(\theta)$ ($f_{\alpha\beta}$ is dimensionless and g_a has dimensions of MPa^{-1}).

θ	g_r (MPa^{-1})	g_θ (MPa^{-1})	f_θ	$f_{r\theta}$	f_{rr}
0	-0.0056	0.2805	0.8160	0.1977	-0.3811
15	0.0191	0.2972	0.6631	0.3854	0.3512
30	0.0528	0.3002	0.4618	0.4060	0.7115
45	0.0867	0.2873	0.2814	0.3054	0.9657
60	0.1123	0.2608	0.1742	0.1169	1.1319
75	0.1239	0.2266	0.1727	-0.1130	1.1934
90	0.1197	0.1924	0.2839	-0.3299	1.1449
91	0.1149	0.1904	0.2948	-0.3328	0.5081
105	0.0448	0.1805	0.4523	-0.3381	0.3798
120	-0.0229	0.2057	0.6061	-0.2723	0.2566
135	-0.0667	0.2601	0.7120	-0.1482	0.1806
150	-0.0753	0.3289	0.7479	0.0048	0.1738
165	-0.0460	0.3935	0.7085	0.1500	0.2415
180	0.0146	0.4364	0.6065	0.2529	0.3711
195	0.0928	0.4452	0.4694	0.2890	0.5349
210	0.1703	0.4156	0.3331	0.2498	0.6971
225	0.2291	0.3526	0.2332	0.1449	0.8221
240	0.2556	0.2690	0.1965	-0.0003	0.8830
255	0.2440	0.1824	0.2344	-0.1509	0.8682
270	0.1976	0.1113	0.3406	-0.2705	0.7844
285	0.1280	0.0702	0.4921	-0.3302	0.6543
300	0.0523	0.0666	0.6549	-0.3156	0.5118
315	-0.0108	0.0988	0.7925	-0.2298	0.3937
330	-0.0460	0.1565	0.8738	-0.0933	0.3308
345	-0.0442	0.2233	0.8817	0.0615	0.3404
360	-0.0056	0.2805	0.8161	0.1977	0.4224

Table A2. Values for the normalized angular shape functions associated to λ_2 in (1) $g_r^2(\theta)$, $g_\theta^2(\theta)$, $f_{\theta\theta}^2(\theta)$, $f_{r\theta}^2(\theta)$ and $f_{rr}^2(\theta)$.

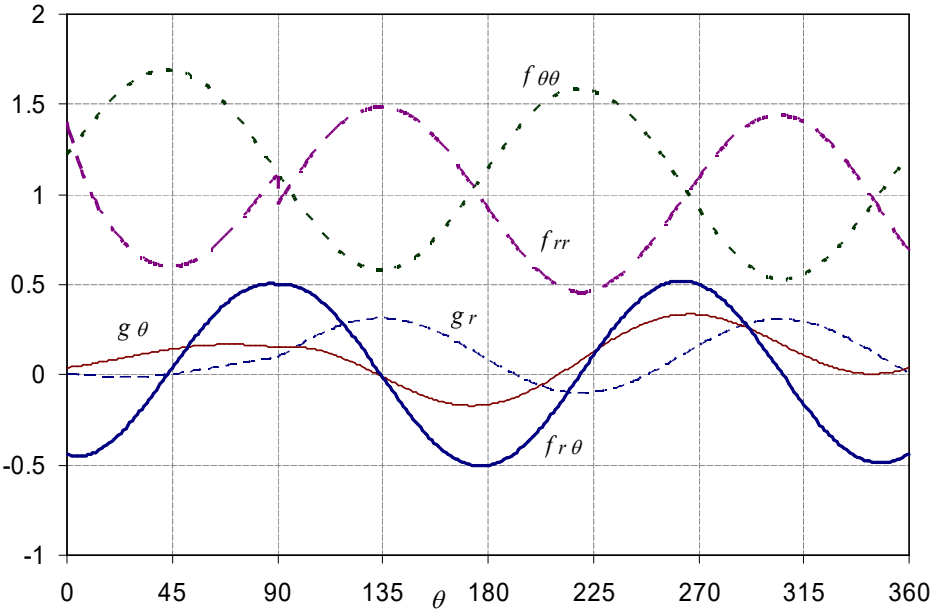

Figure A3. Angular shape functions associated to λ_3 in (1) $g_r^3(\theta)$, $g_\theta^3(\theta)$, $f_{\theta\theta}^3(\theta)$, $f_{r\theta}^3(\theta)$ and $f_{rr}^3(\theta)$ ($f_{\alpha\beta}$ is dimensionless and g_a has dimensions of MPa^{-1}).

θ	g_r (MPa^{-1})	g_θ (MPa^{-1})	$f_{\theta\theta}$	$f_{r\theta}$	f_{rr}
0	0.0058	0.0394	1.2173	-0.4368	1.4042
15	-0.0118	0.0721	1.4598	-0.4072	0.8879
30	-0.0138	0.1100	1.6380	-0.2203	0.6655
45	0.0015	0.1438	1.6895	0.0386	0.6002
60	0.0300	0.1646	1.5968	0.2899	0.6774
75	0.0631	0.1674	1.3847	0.4606	0.8665
90	0.0909	0.1523	1.1126	0.5023	1.1076
91	0.0985	0.1537	1.0941	0.5032	0.9621
105	0.2011	0.1439	0.8446	0.4442	1.2158
120	0.2821	0.0815	0.6472	0.2531	1.4163
135	0.3101	-0.0116	0.5794	-0.0136	1.4856
150	0.2767	-0.1032	0.6615	-0.2765	1.4033
165	0.1918	-0.1614	0.8692	-0.4571	1.1938
180	0.0806	-0.1641	1.1405	-0.5014	0.9191
195	-0.0240	-0.1059	1.3945	-0.3957	0.6601
210	-0.0910	0.0006	1.5550	-0.1711	0.4930
225	-0.1006	0.1285	1.5734	0.1065	0.4664
240	-0.0502	0.2446	1.4429	0.3550	0.5870
255	0.0452	0.3190	1.2008	0.5012	0.8177
270	0.1571	0.3343	0.9170	0.5022	1.0885
285	0.2522	0.2905	0.6737	0.3581	1.3172
300	0.3019	0.2052	0.5409	0.1122	1.4339
315	0.2914	0.1082	0.5553	-0.1623	1.4018
330	0.2234	0.0328	0.7100	-0.3834	1.2278
345	0.1179	0.0057	0.9561	-0.4851	0.9610
360	0.0058	0.0394	1.2173	-0.4368	0.6776

Table A3. Values for the normalized angular shape functions associated to λ_3 in (1) $g_r^3(\theta)$, $g_\theta^3(\theta)$, $f_{\theta\theta}^3(\theta)$, $f_{r\theta}^3(\theta)$ and $f_{rr}^3(\theta)$.